

## Synthesis and optical characterization of porous ZnO

K. SOWRI BABU\*, A. RAMACHANDRA REDDY, Ch. SUJATHA,  
K. VENUGOPAL REDDY, A. N. MALLIKA

*Department of Physics, National Institute of Technology Warangal, Warangal-506 004, Andhra Pradesh, India*

Received: March 18, 2013; Revised: April 19, 2013; Accepted: May 03, 2013

©The Author(s) 2013. This article is published with open access at Springerlink.com

**Abstract:** In this paper, a simple and cheap method to prepare porous ZnO by using zinc nitrate, ethanol and triethanolamine (TEA) is reported. The as-prepared sample consisted of nano and micro pores. The sample was calcined at 300 °C, 400 °C and 500 °C with different heating rates. At 500 °C, the nano pores disappeared but the sample maintained its micro porosity. Field emission scanning electron microscopy (FE-SEM) pictures confirmed that the size and growth of ZnO nanoparticles depended on the heating conditions. The infrared (IR) absorption peak of Zn–O stretching vibration positioned at 457 cm<sup>-1</sup> was split into two peaks centered at 518 cm<sup>-1</sup> and 682 cm<sup>-1</sup> with the change of morphology. These results confirmed that Fourier transform infrared (FT-IR) spectrum was sensitive to variations in particle size, shape and morphology. The photoluminescence (PL) spectrum of porous ZnO contained five emission peaks at 397 nm, 437 nm, 466 nm, 492 nm and 527 nm. Emission intensity enhanced monotonously with increase of temperature and the change was rapid between temperatures of 300 °C and 500 °C. This was due to the elimination of organic species and improvement in the crystallinity of the sample at 500 °C.

**Keywords:** semiconductors; porous ZnO; optical properties

### 1 Introduction

Materials exhibit novel and fascinating properties with reduction of size from bulk to nanometer scale. As far as the semiconductor nanoparticles are concerned, the increase in band gap has been observed when the particle size is comparable to or smaller than the excitonic Bohr radius. Consequently, the emission spectrum shows blue shift (shift towards lower wavelength) and it is called quantum confinement effect. Among the various known semiconductors, ZnO has several advantages compared to other

wide-band-gap semiconductors. It has a direct band gap of 3.37 eV and large exciton binding energy of 60 meV at room temperature [1]. Due to these unique properties, it finds applications in antireflection coatings, transparent electrodes in solar cells, ultraviolet (UV) light emitters, diode lasers, varistors, piezoelectric devices, spin-electronics, surface acoustic wave propagation, and also in sensing of gas [2]. It is well known that nanostructures have very good sensitivity with respect to size, shape, type of material and preparation techniques. In the case of ZnO, it is able to satisfy above properties because it can be easily synthesized in various shapes like particles, rods, needles, shells, tubes, wires, nails, belts, combs, propellers, springs, tetrapods, etc. [3–8].

Apart from the above variety of structures, porous

\* Corresponding author.

E-mail: sowribabuk@gmail.com

ZnO can also be prepared. Porous ZnO has some specific advantages such as high surface area, chemical and photochemical stability, uniformity in pore size, shape selectivity, and rich surface chemistry [9]. The high surface area of porous ZnO makes its surface more active. The highly active surface would increase the probability of interaction of gases with the semiconductor, which in turn increases the sensitivity of the material [10]. So, the material has found a variety of promising applications such as catalysts, nano-sieve filters, dye sensitized solar cells, bio- and electrochemical sensors, bone-replacement materials and also in gas sensors [9,11,12]. For example, for dye sensitized solar cells, ZnO thin films should be porous and have high specific surface area for obtaining high conversion efficiency of light into current [13]. Recently, some attention has been paid to the synthesis of porous ZnO by using various methods such as thermal decomposition method, template assisted methods, hydrothermal method, solid-vapor process, radio frequency sputtering, electrochemical deposition, etc. [13–15]. To the best of our knowledge, an easy and economical method to prepare porous ZnO is not addressed so far. So, because of the importance of porous ZnO in various applications mentioned above, the following work is taken up.

In this work, a simple and cheap method to prepare nanoporous ZnO using zinc nitrate, ethanol and triethanolamine (TEA) is reported. The as-prepared sample was calcined at 300 °C, 400 °C and 500 °C and studied with their structural and optical properties. The sample was characterized with X-ray diffraction (XRD), field emission scanning electron microscopy (FE-SEM), ultraviolet–visible (UV–Vis) spectrophotometer, and Fourier transform infrared (FT-IR) and photoluminescence (PL) spectrometers to study their structural and optical properties.

## 2 Experimental procedures

The preparation of porous ZnO is as follows. 0.53 g of  $\text{Zn}(\text{NO}_3)_2 \cdot 6\text{H}_2\text{O}$  was dissolved in ethanol and stirred on magnetic hot plate until it became clear and stable. To this solution, a few drops of TEA were added and stirring was continued for one more hour at room temperature. In the next step, the temperature of the hot plate was increased to 80 °C to evaporate the solvent. Then, the solution was converted into a gel. The gel was subsequently swelling into foam and

underwent a self-propagating combustion reaction on the hot plate itself to give fine powder. The combustion took place within few seconds and the resulted powder was of dark brown color. Afterwards, the sample was calcined at 300 °C and 500 °C with a heating rate of 2 °C/min in a programmable furnace. As the temperature was increased to 500 °C, the color of the sample changed from brown to white. To know the influence of heating conditions on the size of the particles and growth, the sample was also calcined at 400 °C with a heating rate of 1 °C/min.

XRD measurements were taken on Inel XRG 3000 diffractometer equipped with Cobalt  $K\alpha$  ( $\lambda = 1.78897 \text{ \AA}$ ) radiation (15 mA, 30 kV). The morphology of the sample was studied by using ZEISS FE-SEM. Absorption spectra were acquired on Analyticazena (Specord 205) UV–Vis spectrophotometer. FT-IR spectra of the sample were recorded on Bruker Optics FT-IR Spectrometer Model: Tensor 27. PL measurements were performed on Jobin Yuon spectrofluorometer with 450 W xenon arc lamp.

## 3 Results and discussion

### 3.1 XRD analysis

Figure 1 shows the XRD patterns for the as-prepared porous ZnO and porous ZnO calcined at 300 °C and 500 °C. This picture depicts the characteristic peaks (100), (002), (101), (102), (110), (103), etc., which correspond to the wurtzite ZnO structure. The broadening of these peaks decreases continuously, which is an indication of the increase in particle size and improved crystallinity with a rise of temperature. The change is drastic as the temperature increases from 300 °C to 500 °C. The crystallite size of the sample is calculated using Debye–Scherrer formula:

$$D = \frac{0.9\lambda}{\beta \cos \theta}$$

where  $D$  is the particle diameter;  $\lambda$  is the wavelength of the X-ray used;  $\beta$  is the FWHM (full width at half maximum); and  $\theta$  is the diffraction angle. The crystallite size values for the as-prepared porous ZnO and the samples calcined at 300 °C and 500 °C are 3 nm, 6 nm and 43 nm, respectively. This drastic change in crystallite size indicates that up to 300 °C only the progress of crystallization from amorphous state occurs and further growth takes place above

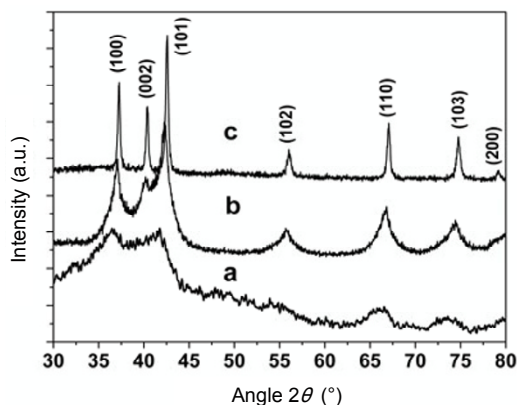


Fig. 1 Typical XRD patterns of (a) the as-prepared porous ZnO and porous ZnO annealed at (b) 300 °C and (c) 500 °C.

300 °C. Hence well crystallized ZnO is formed at 500 °C and the color of the sample turns out from brown to white. It can also be seen from Fig. 1 that diffraction peaks of ZnO shift towards the higher angle side compared to the as-prepared porous ZnO with a rise of temperature. This implies that ZnO nanoparticles are under compressive stress.

### 3.2 FE-SEM analysis

The FE-SEM micrographs of the as-prepared porous ZnO and porous ZnO annealed at 500 °C are presented in Fig. 2. The as-prepared sample contains nano and micro pores with diameters ranging from a few nanometers to micrometers. The porous ZnO is shown in Fig. 2(b) representing the nano pores. But, such nano pores are not detected when it is calcined at 500 °C. From the FE-SEM micrograph in Fig. 2(d), the average particle size of the porous ZnO calcined at 500 °C comes out to be 47 nm. This value is in good agreement with the value obtained from the XRD data.

### 3.3 UV-Vis analysis

The UV-Vis absorbance spectra of the as-prepared porous ZnO and samples annealed at 300 °C and 500 °C are shown in Fig. 3. The as-prepared porous ZnO depicts an absorption at 347 nm, which is blue shifted compared to the bulk ZnO whose absorption edge is observed at 380 nm. With an increase in temperature, there is a systematic shift in the absorption edge towards higher wavelength side but the maximum shift occurs between temperatures of 300 °C and 500 °C. The absorption edge values corresponding to the samples annealed at 300 °C and

500 °C are 355 nm and 370 nm. This gradual red shift of absorption edge with increase in annealing temperature is obviously due to the increase of particle size. This indicates the strong quantum confinement effects of the porous ZnO nanoparticles. The particle size has also been calculated from the absorption edge values of all the three samples according to Ref. [2]. The effective mass model has been used for finding particle size of ZnO nanoparticles. This model utilizes the fact that the wavelength of absorption depends on particle size. The particle sizes obtained for all the three samples are 5 nm, 7 nm and 13 nm, respectively. The particle size values for the as-prepared sample and sample calcined at 300 °C are in good agreement with the values measured from XRD. But in the case of

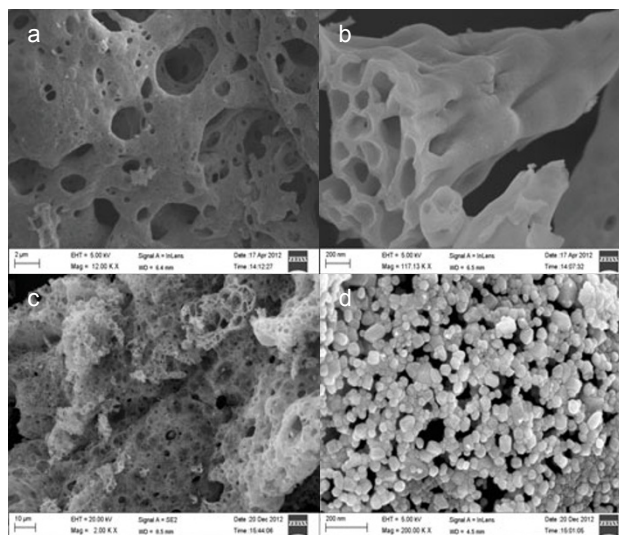


Fig. 2 FE-SEM pictures of the as-prepared porous ZnO ((a) and (b)) and porous ZnO annealed at 500 °C ((c) and (d)).

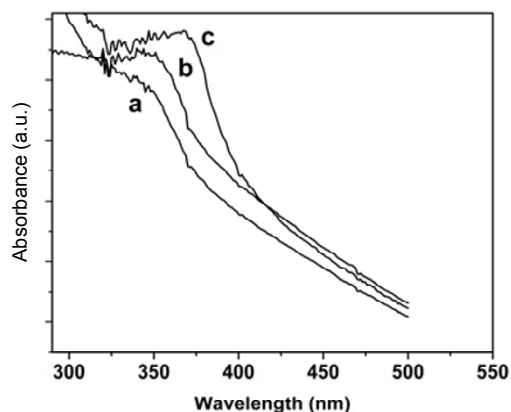


Fig. 3 UV-Vis absorption spectra of (a) the as-prepared porous ZnO and porous ZnO calcined at (b) 300 °C and (c) 500 °C.

the sample calcined at 500 °C, the particle size calculated from UV–Vis absorbance spectrum is not coinciding with the results obtained from FE-SEM and XRD.

### 3.4 FT-IR analysis

The FT-IR spectra of the samples measured in the range of 4000–400  $\text{cm}^{-1}$  are presented in Fig. 4. The as-prepared ZnO shows IR peaks at 457  $\text{cm}^{-1}$ , 1063  $\text{cm}^{-1}$ , 1390  $\text{cm}^{-1}$ , 1602  $\text{cm}^{-1}$  and 3423  $\text{cm}^{-1}$ . The sharp peak positioned at 457  $\text{cm}^{-1}$  is attributed to the Zn–O stretching bonds. The IR bands shown in Fig. 4 are in the region of 1700–600  $\text{cm}^{-1}$  and correspond to C=O, C–O and C–H vibrations respectively [16]. Remaining peaks are due to the O–H stretching vibrations and bending modes of the adsorbed water. With the increase of temperature, the intensity of peaks centered at 1063  $\text{cm}^{-1}$ , 1390  $\text{cm}^{-1}$  and 1602  $\text{cm}^{-1}$  are deteriorated and at 500 °C these peaks are almost disappeared. It indicates that organic species are completely removed at 500 °C. It is observed that the position of 457  $\text{cm}^{-1}$  peak remains the same when annealed at 300 °C but shifts to 439  $\text{cm}^{-1}$  at 500 °C. The shift of the XRD peaks is also observed between 300 °C and 500 °C, which is attributed to the compressive stress acting on ZnO nanoparticles. So, the broadening and shift of the IR peak to lower wavenumber could be due to the stress acting on ZnO nanoparticles and variation in morphology. Figure 4(b) shows the FT-IR spectrum of porous ZnO calcined at

400 °C at a heating rate of 1 °C/min along with its FE-SEM micrograph. It is apparent from the micrograph that the initial particles are spherical in shape with an approximate size of 9 nm. This size seems to be critical and if once reaching that size, they tend to agglomerate to bigger particles. These nanoparticles grow to larger sizes at the expense of other small particles through Ostwald ripening process. Interestingly, the sharp peak at 457  $\text{cm}^{-1}$  splits into two peaks positioned at 518  $\text{cm}^{-1}$  and 682  $\text{cm}^{-1}$ . Similar results are observed in the case of ZnO microcrystals and the position of the peaks is dependent on axial ratio ( $c/a$ ) of the crystals [17]. The FE-SEM picture of this sample shows the change of morphology of ZnO nanoparticles from spherical to cylinder shape, so the splitting of Zn–O stretching band in FT-IR spectrum can be assigned to the change in morphology of ZnO nanoparticles. It is obvious from FT-IR spectrum of porous ZnO calcined at 400 °C at a heating rate of 1 °C/min that organic species are not eliminated at this temperature.

### 3.5 PL analysis

Room-temperature PL spectra of the samples recorded at an excitation wavelength of 320 nm are shown in Fig. 5. All the samples exhibit near UV emission at around 397 nm and four defect related peaks at 437 nm, 466 nm, 492 nm and 527 nm. The intensity of all these emission peaks is enhanced with the rise of temperature. It can be seen from the figure that there is no significant change in the emission intensities of the

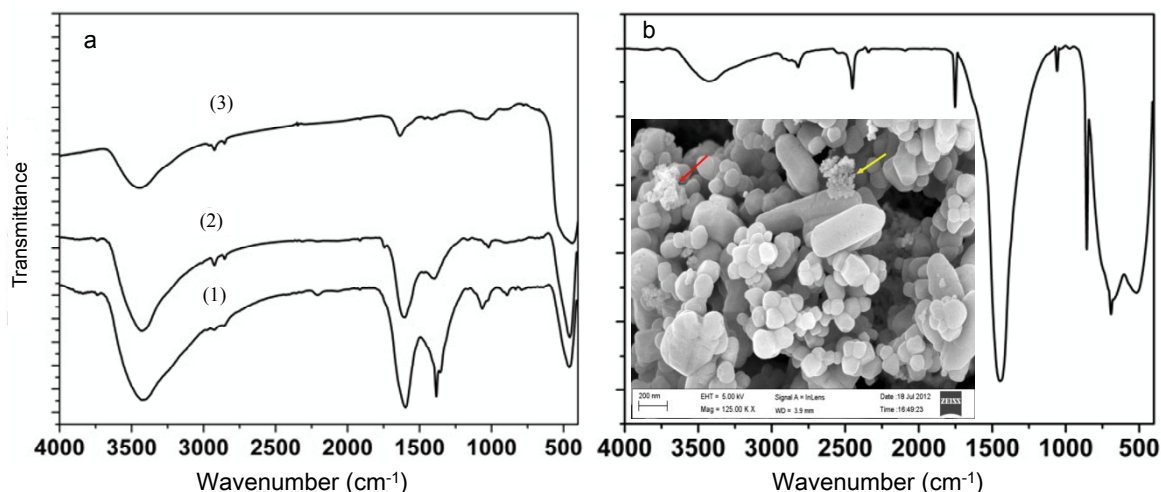


Fig. 4 (a) FT-IR spectra of (1) the as-prepared porous ZnO and porous ZnO calcined at (2) 300 °C and (3) 500 °C; (b) FT-IR spectrum of the sample calcined at 400 °C with a heating rate of 1 °C/min and inset shows the FE-SEM picture of the sample.



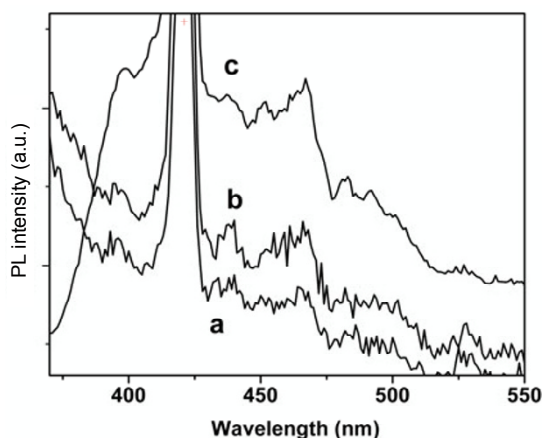


Fig. 5 PL spectra of (a) the as-prepared porous ZnO and porous ZnO calcined at (b) 300 °C and (c) 500 °C.

as-prepared porous ZnO and porous ZnO calcined at 300 °C. But when the temperature is increased to 500 °C, the intensities of emission peaks are enhanced remarkably. Very recently, it was proved that 398 nm peak is originated from the electron transition from the localized level, slightly below conduction band to the valence band [18]. The enhanced intensity of these emission peaks is obviously due to the improved crystallinity of the ZnO with rise of temperature as confirmed from XRD, FE-SEM and UV-Vis results. The enhancement of the defect related emission intensities along with the UV emission indicates that these defects are intrinsic in nature. The emission peak at 437 nm can be attributed to the zinc vacancy [19]. The other visible emission peaks at 466 nm, 492 nm and 527 nm have been assigned to various deep level defect states originated from the zinc interstitials and/or oxygen vacancies [5,19].

## 4 Conclusions

Porous ZnO was synthesized by a simple method using zinc nitrate, ethanol and TEA. The as-prepared sample contained both nano and micro pores. The nano pores were disappeared but microporosity of the sample was retained even at 500 °C. It was found that the shape of the FT-IR spectrum depends on the size and morphology of ZnO nanoparticles. The stress and change in morphology were responsible for the shift of Zn–O stretching mode to lower wavenumber side. The absorption spectra showed continuous red shift from 347 nm to 370 nm with rise of temperature. PL

emission intensity enhanced with increase of temperature. The near UV emission at 397 nm has been attributed to the electron transition from the localized level slightly below conduction band to the valence band. The visible emission at 437 nm was attributed to the zinc vacancy. The other visible emissions at 466 nm, 492 nm and 527 nm were assigned to the zinc interstitials and/or oxygen vacancies.

## Acknowledgements

The authors thank the dean of School of Physics, University of Hyderabad, for providing FE-SEM facility generously, and are also grateful to Y. B. Ravi Shankar for his continuous support in XRD analysis of the samples.

**Open Access:** This article is distributed under the terms of the Creative Commons Attribution Noncommercial License which permits any noncommercial use, distribution, and reproduction in any medium, provided the original author(s) and source are credited.

## References

- [1] Service RF. Will UV lasers beat the blues? *Science* 1997, **276**: 895.
- [2] Singh AK, Viswanath V, Janu VC. Synthesis, effect of capping agents, structural, optical and photoluminescence properties of ZnO nanoparticles. *J Lumin* 2009, **129**: 874–878.
- [3] Koch U, Fotik A, Weller H, *et al.* Photochemistry of semiconductor colloids. Preparation of extremely small ZnO particles, fluorescence phenomena and size quantization effects. *Chem Phys Lett* 1985, **122**: 507–510.
- [4] Djurišić AB, Leung YH, Tam KH, *et al.* Green, yellow, and orange defect emission from ZnO nanostructures: Influence of excitation wavelength. *Appl Phys Lett* 2006, **88**: 103107.
- [5] Jamali-Sheini F. Chemical solution deposition of ZnO nanostructure films: Morphology substrate angle dependency. *Ceram Int* 2012, **38**: 3649–3657.
- [6] Wei A, Sun XW, Xu CX, *et al.* Growth mechanism of tubular ZnO formed in aqueous solution. *Nanotechnology* 2006, **17**: 1740–1744.
- [7] Wu L, Wu Y, LÜ W. Preparation of ZnO nanorods and optical characterizations. *Physica E* 2005, **28**:

- 76–82.
- [8] Roy VAL, Djurišić AB, Chan WK, *et al.* Luminescent and structural properties of ZnO nanorods prepared under different conditions. *Appl Phys Lett* 2003, **83**: 141–143.
- [9] Kılıç B, Gür E, Tüzemen S. Nanoporous ZnO photoelectrode for dye-sensitized solar cell. *J Nanomater* 2012, DOI: 10.1155/2012/474656.
- [10] Li B, Wang Y. Hierarchically assembled porous ZnO microstructures and applications in a gas sensor. *Superlattice Microst* 2011, **49**: 433–440.
- [11] Jeon SM, Kim MS, Cho MY, *et al.* Fabrication of porous ZnO nanorods with nano-sized pores and their properties. *J Korean Phys Soc* 2010, **57**: 1477–1481.
- [12] Dai Z, Liu K, Tang Y, *et al.* A novel tetragonal pyramid-shaped porous ZnO nanostructure and its application in the biosensing of horseradish peroxidase. *J Mater Chem* 2008, **18**: 1919–1926.
- [13] Liu Z, Jin Z, Li W, *et al.* Preparation of porous ZnO plate crystal thin films by electrochemical deposition using PS template assistant. *Mater Lett* 2006, **60**: 810–814.
- [14] Li S, Zhang X, Jiao X, *et al.* One-step large-scale synthesis of porous ZnO nanofibers and their application in dye-sensitized solar cells. *Mater Lett* 2011, **65**: 2975–2978.
- [15] Ching CG, Ooi PK, Ng SS, *et al.* Fabrication of porous ZnO via electrochemical etching using 10 wt% potassium hydroxide solution. *Mat Sci Semicon Proc* 2013, **16**: 70–76.
- [16] Xiong H-M, Shchukin DG, Möhwald H, *et al.* Sonochemical synthesis of highly luminescent zinc oxide nanoparticles doped with magnesium(II). *Angew Chem Int Edit* 2009, **48**: 2727–2731.
- [17] Andrés Vergés M, Mifsud A, Sernad CJ. Formation of rod-like zinc oxide microcrystals in homogeneous solutions. *J Chem Soc Faraday Trans* 1990, **86**: 959–963.
- [18] Sowri Babu K, Ramachandra Reddy A, Sujatha Ch, *et al.* Optimization of UV emission intensity of ZnO nanoparticles by changing the excitation wavelength. *Mater Lett* 2013, **99**: 97–100.
- [19] Giri PK, Bhattacharyya S, Singh DK, *et al.* Correlation between microstructure and optical properties of ZnO nanoparticles synthesized by ball milling. *J Appl Phys* 2007, **102**: 093515.